

Accurate Determination of Structure Factors by Pendellosung Methods using White Radiation*

T. Takama and S. Sato

Department of Applied Physics, Faculty of Engineering,
Hokkaido University, Sapporo 060, Japan.

Abstract

This paper describes two experimental techniques measuring the Pendellösung beats using white radiation, developed in the authors' laboratory. The intensity of a Laue spot diffracted from a parallel-sided single crystal is successively measured at different Bragg angles, i.e. with different wavelengths. The values of structure factors are evaluated from extremum positions in the measured beats on the basis of the dynamical diffraction theory. In the first method, the integrated intensity diffracted from the whole exit surface is measured, and in the second, the measurement is made only at the centre of the Borrmann fan on the exit surface of a specimen. A discussion is given on the accuracy associated with the following origins of errors: (1) polarisation of incident white radiation, (2) measurement of specimen thickness, (3) measurement of wavelength, (4) determination of extremum positions, and (5) effect of defects in the crystal.

1. Introduction

Based upon the dynamical theory of X-ray diffraction, structure factors can be determined experimentally by measuring the spacing of the Pendellösung fringes. The fringes have usually been observed on topographs using characteristic X rays and wedge-shaped perfect single crystals. Kato and Lang (1959) first observed the fringes on the topograph to measure the structure factors of Si and other materials and many workers have applied this technique for evaluating the structure factors of various materials. The method requires accurate collimation of characteristic X rays and precise shaping of a large single crystal.

The Pendellösung fringes have also been observed in the topographic image of white radiation (Hashimoto *et al.* 1965; Kozaki *et al.* 1968; Aristov *et al.* 1977). These fringes are apparently produced by the change in extinction distance with wavelength of diffracted X rays. Aristov *et al.* measured the structure factors of Si and Ge using white X-ray topographs from parallel-sided and wedge-shaped specimens. In this case it is rather difficult to determine an accurate wavelength corresponding to a position on the topograph.

The present authors have lately proposed two experimental techniques in which the Pendellösung intensity beats are directly measured with respect to the wavelength using white radiation and the energy-dispersive diffraction method. In the first technique, Method 1, the integrated intensity of a whole Laue spot diffracted from a

* Paper presented at the International Symposium on Accuracy in Structure Factor Measurement, held at Warburton, Australia, 23–26 August 1987.

parallel-sided single crystal specimen is measured at different angles. The technique has already been applied to obtain accurate structure factors of Si (Takama *et al.* 1980), Ge (Takama and Sato 1981), Cu (Takama and Sato 1982), Al (Takama *et al.* 1982), Zn (Takama *et al.* 1984*a*), and diamond, α -quartz, GaAs and InP (Takama *et al.* 1984*b*).

In the second Method 2 (Takama *et al.* 1983) the diffracted intensity from the exit surface of a thick crystal is measured only at the centre of the Borrmann fan. Since the beats are not only of large amplitude but also of high frequency, the accuracy in structure factor determination is remarkably improved in Method 2.

Both these techniques possess various advantages as described below. In this report, the basic principle and the system of measurement in these techniques are described in detail. Moreover, some of the results obtained have been compared with previously reported values and the errors possibly introduced from various causes are discussed as well.

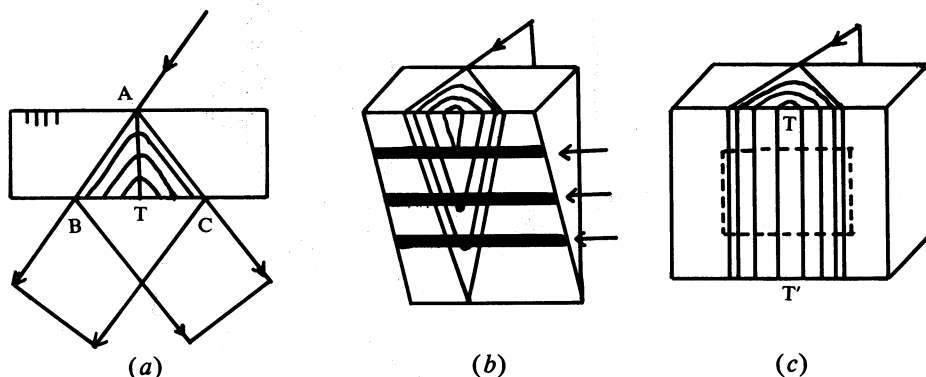


Fig. 1. (a) Hyperbolic equi-intensity wave field in the Borrmann fan. (b) Bamboo-shoot type intensity distribution on the exit surface of wedge-shaped crystal. The arrows correspond to the thickness fringes on the transverse topograph. (c) Parallel intensity distribution on the exit surface of parallel-sided crystal. Method 1: Intensity from dashed square is measured. Method 2: Intensity from TT' is measured.

2. Principle of Measurement

When a strong Bragg reflection takes place, two waves propagating in the transmitted and diffracted directions are excited in the crystal. Each is known to be composed of two Bloch waves with slightly different wave vectors, which interfere on propagation to produce an oscillatory field, called a 'Pendellösung beat', in the crystal.

The spherical wave dynamical theory (Kato 1961, 1968*a*) predicts that a hyperbolic equi-intensity wave field appears in the Borrmann fan ABC, as shown schematically in Fig. 1*a*. As seen in Figs 1*b* and 1*c*, bamboo-shoot shaped and parallel interference beats are formed at the exit surface of wedge-shaped and parallel-sided crystals respectively.

The period of oscillation along AT in Fig. 1*a* is called the extinction distance, which can be expressed as a function of the structure factor. Accordingly, one

evaluates the structure factor by taking a topograph corresponding to Fig. 1*b* and measuring the fringe spacing. This is the method called 'section topograph' and Kato and Lang (1959) first observed the fringes. When the wedge-shaped specimen is horizontally transversed simultaneously with the photographic plate, the thickness extinction fringe pattern will be photographed as shown in Fig. 1*b* by the arrows. This is the 'transverse topograph' and the spacing of the fringes has also been measured to evaluate the structure factors.

On the other hand, since the extinction distance is inversely proportional to the wavelength, the number of beats increases with increasing wavelength. Therefore, a similar fringe pattern can be observed on the topograph when the parallel-sided specimen is irradiated by white radiation.

In the present technique, Method 1, instead of taking topographs, the integrated intensity diffracted from the region surrounded by the dashed line in Fig. 1*c* is successively measured by a solid state detector with different Bragg angles. The whole intensity of a Laue spot is integrated and hence this method is thought to correspond to the transverse topograph. Contrary to this, the intensity diffracted only from TT' in Fig. 1*c* is measured with different wavelengths in Method 2, which corresponds to the section topograph of characteristic X rays.

3. Method 1

(a) Integrated Intensity

According to the dynamical theory of X-ray diffraction with absorption, the integrated intensity J_{hkl} in the symmetrical Laue case can be expressed, assuming unpolarised incident radiation, as follows (Kato 1955, 1968*b*; DeMarco and Weiss 1965; Buras *et al.* 1975):

$$J_{hkl} = K I_e(E) |F'_{hkl}| (R_{hkl,n} + |\cos 2\theta| R_{hkl,p}) / \sin \theta, \quad (1)$$

where

$$R_{hkl,n,p} = \frac{1}{2} \pi \exp\{-\mu(E)t/\cos \theta\} \times \left(\int_0^{2A_{n,p}} J_0(x) dx + I_0(2i|k|A_{n,p}) - 1 \right), \quad (2)$$

$$A_{n,p} = (e^2/mc^2)(\lambda t/\cos \theta) |F'_{hkl}| C_{n,p}/V, \quad (3)$$

and K is a constant depending on the experimental conditions, $I_e(E)$ is the incident beam spectrum, θ is the Bragg angle, t is the specimen thickness, $\mu(E)$ is the linear absorption coefficient, E is the photon energy, J_0 is the Bessel function of zeroth order, I_0 is the modified Bessel function, e^2/mc^2 is the classical electron radius, V is the volume of the unit cell, and $C_{n,p}$ is the polarisation factor, with n and p referring to normal and parallel polarisation components of X rays respectively. The structure factor is

$$\begin{aligned} F_{hkl} &= F'_{hkl} + i F''_{hkl} \\ &= \sum_j (f_{hkl}^0 + f' + i f'')_j \exp(-M_j) \exp(2\pi i H_{hkl} r_j), \end{aligned}$$

and $|k| = |F''_{hkl}|/|F'_{hkl}|$, with $\exp(-M_j) = \exp(-B_j \sin^2 \theta/\lambda^2)$ a temperature factor.

The integral of the zeroth order Bessel function appearing in equation (2) oscillates with $A_{n,p}$, i.e. with t when $\lambda/\cos\theta$ is constant or with $\lambda/\cos\theta$ when t is constant. The former case corresponds to the usual Pendellösung fringes due to the thickness change of the specimen appearing in topographs taken by characteristic radiation. The latter corresponds to the present method using a parallel-sided specimen where the extremum positions of the beats are measured as a function of the X-ray wavelength and the structure factor $|F'_{hkl}|$ can be determined with its wavelength dependence.

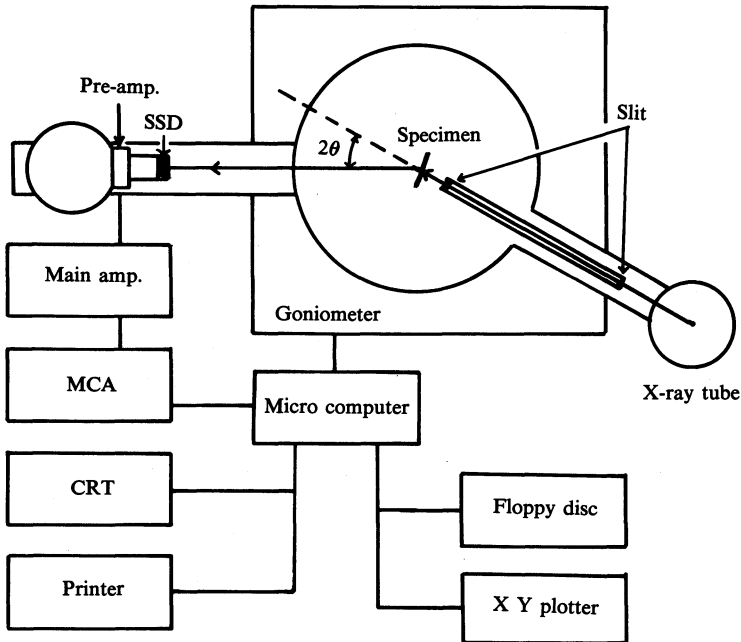


Fig. 2. Experimental arrangement of Method 1.

(b) Measurement of Beats

Parallel-sided single crystals with high perfection are to be used in this measurement. For semiconductors such as Si, Ge, etc. the technique of growing single crystals has developed remarkably and, moreover, not much caution has to be paid to shaping these materials in the parallel-sided form. However, for soft materials such as Cu, Al, Zn, etc. it is almost impossible to handle these crystals mechanically without introducing lattice imperfections. Therefore, a method without shaping after growing single crystals is necessary for these materials. We have tried whiskers of Cu, annealed Al wafers and as-grown sheets of Zn, and succeeded in obtaining clear Pendellösung beats by collimating a white X-ray beam so as to hit only an area free from dislocations or any other irregularities introduced during the crystal growth.

Fig. 2 illustrates the measuring system of Method 1. White radiation from an X-ray tube falls on an area of the specimen through a slit system. A certain slit size is selected depending upon the size or quality of the specimen. Fig. 3 shows

an example of transmission white X-ray topographs of a synthetic diamond wafer showing grown-in dislocations. The black square area is set exactly at the centre of a single crystal goniometer, being irradiated by X rays. The X rays diffracted through the specimen at an angle 2θ are energy-analysed using a solid-state detector (SSD) of intrinsic Ge and a multichannel pulse height analyser (MCA). The photon energy which corresponds to the MCA channel number is calibrated by using various γ -ray and X-ray emission lines of several elements. The value of J_{hkl} is obtained after subtracting the background intensity from the measured intensity distribution. The variation of J_{hkl} with respect to the photon energy or wavelength λ is obtained by repeating the same measurement at different θ - 2θ positions under computer control.

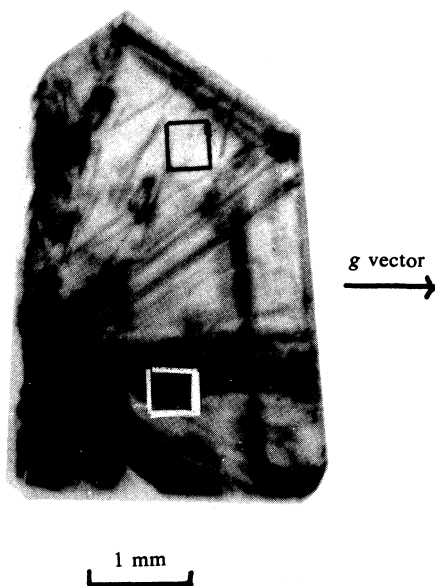


Fig. 3. Transmission white X-ray topograph of a synthetic diamond. The black square shows the irradiated area in Method 1. A similar measurement was made for the region marked by the white square.

(c) Corrections and Analysis

Fig. 4 shows an example of the measured Pendellösung beats for the 111 reflection diffracted from the region marked by the black square in Fig. 3. A fading region, where the two beats with normal and parallel components of polarisation having different periods superpose to produce a fade-out phenomenon, can be seen at about $\lambda = 0.75 \text{ \AA}$. The as-measured curves are subjected to several corrections in order to make the true Pendellösung beats clearer. The spectrum of the incident radiation $I_c(E)$ is determined by measuring the intensity of the 220 reflection from a thick Si single crystal. The experimental arrangement and procedure are the same as the main experiment for obtaining the Pendellösung intensity beats, except that the Si crystal is placed in the symmetrical Bragg setting. The intensity equation derived by DeMarco and Weiss (1965) in the Bragg case is utilised to calculate $I_c(E)$ by substituting the structure factor (Hattori *et al.* 1965), assuming unpolarised incident radiation. The Hönl formula (James 1967) for the anomalous dispersion as well as the Victoreen equation ('International Tables for X-ray Crystallography' 1962) for the mass absorption correction are also applied to evaluate $I_c(E)$.

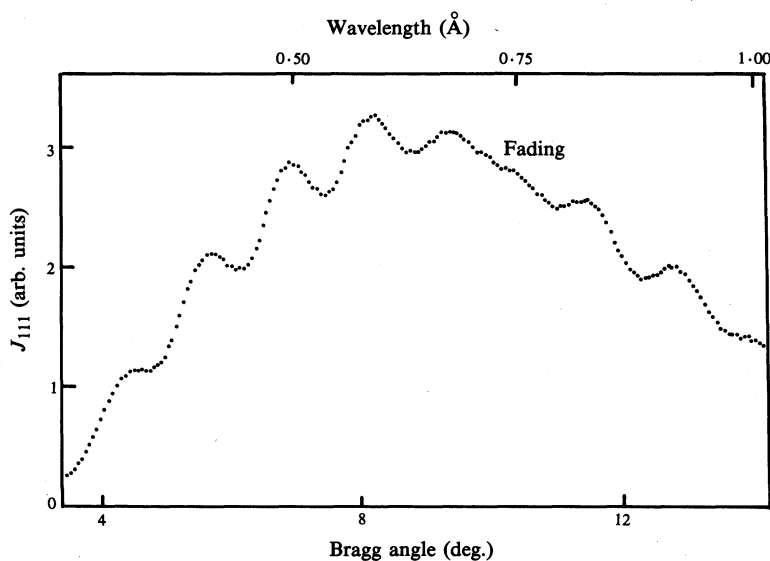


Fig. 4. Measured Pendellösung beats of the 111 reflection of diamond.

The resultant beats obtained from J_{hkl} in Fig. 4 after the corrections for $I_e(E)$ and the absorption and geometrical factors are shown in Fig. 5. Similar beats for Al, Si, Cu and Ge are represented in Fig. 6. One clearly sees that a tendency towards increasing average intensity with wavelength predominates as the atomic number increases. This is because the wavelength range approaches the K absorption edge for the heavy atoms. The increase mainly corresponds to the term $I_0(2i|k|A_{n,p})$ in equation (2). Therefore, especially for heavy atoms, the correction concerning the I_0 term should be made prior to the determination of the extremum positions of beats. Fig. 7 shows an example of the resultant beats corresponding only to the Waller integral, which has been obtained for the 111 reflection of Cu after subtracting the I_0 term calculated by Cromer's (1965) equation for f'' and B (Batterman *et al.* 1961). Fig. 8 shows a diagram relating $|F'_{111}| t$ to λ and θ , on which the extremum positions calculated by the Waller integral in equation (2) are drawn as a series of lines. The measured extremum positions of λ in Fig. 5 are marked by crosses in Fig. 8. If one measures the thickness of the specimen, the structure factor $|F'_{111}|$ can be determined from the ordinate values of these crosses.

The thickness of parallel-sided specimens has been measured by two different methods, depending upon the mechanical nature of material. When the material is hard enough to handle, it is directly measured by a high precision micrometer. For soft metals such as Al, Cu and Zn, an alternative method of measuring the attenuation of characteristic X rays transmitted through the specimen is utilised. The intensity of the monochromatised beam passing through the slit system on the goniometer of the main experiment is measured at the $\theta = 0$ position with and without the specimen in position. The beam intensity is usually fixed as low as possible in order to minimise the counting loss in the SSD.

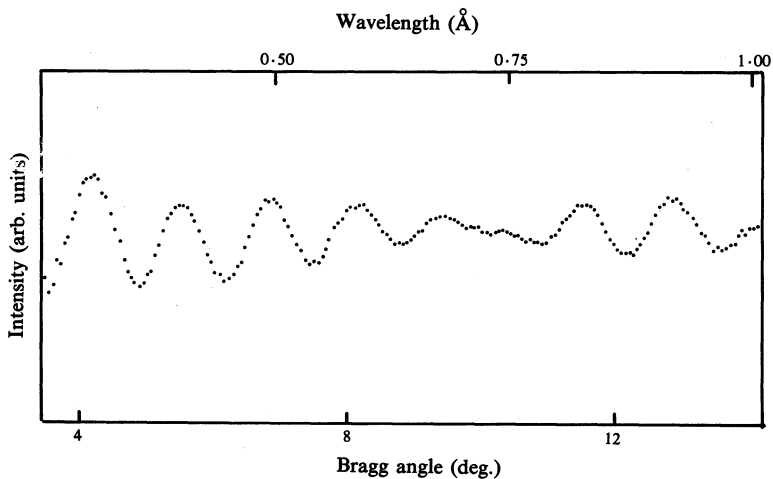


Fig. 5. Pendellösung beats for the 111 reflection of diamond, corrected for $I_e(E)$ and the absorption and geometrical factors.

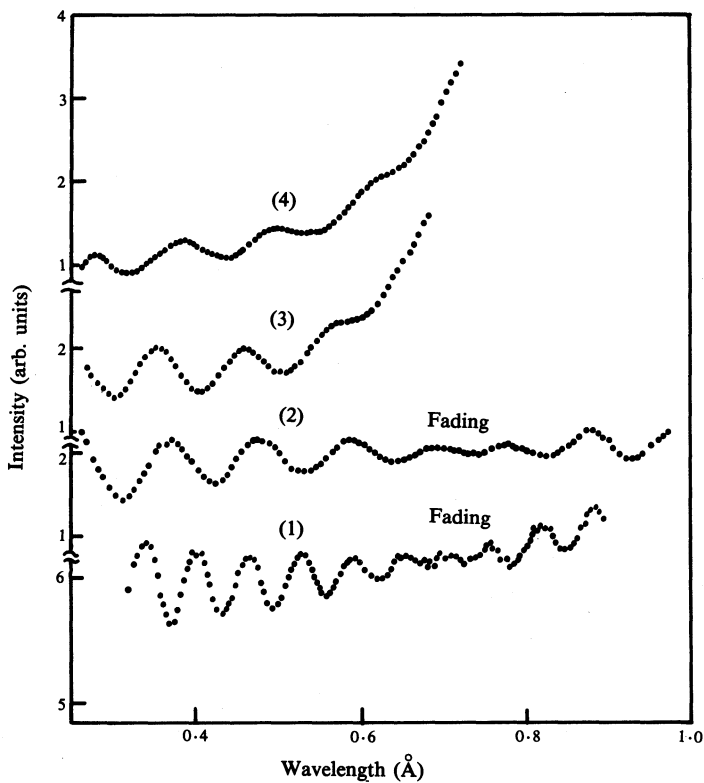


Fig. 6. Examples of beats corrected for $I_e(E)$ and the absorption and geometrical factors: (1) Al 111; (2) Si 220; (3) Cu 220; and (4) Ge 111.

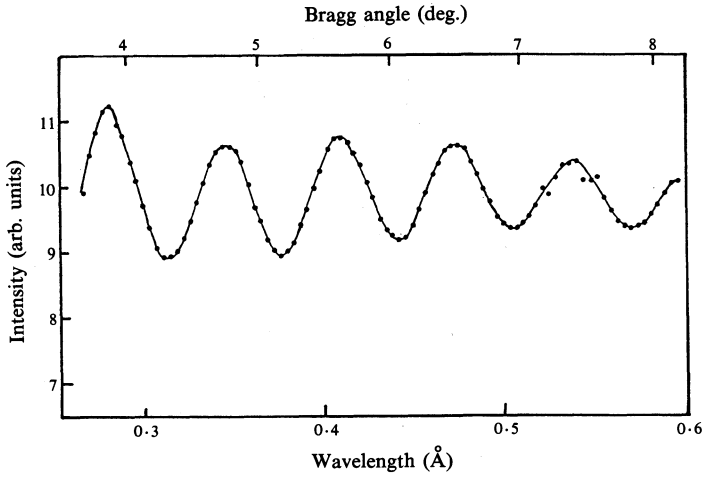


Fig. 7. Example of true Pendellösung beats corresponding to the Waller integral for the Cu 111 reflection.

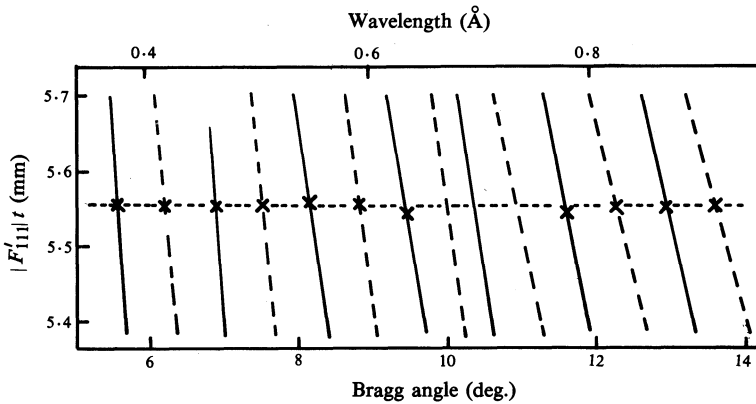


Fig. 8. Calculated maximum (solid lines) and minimum (dashed lines) positions in the beats for the 111 reflection of diamond. The observed positions in Fig. 5 are plotted by crosses. The dotted line connecting the observed positions is almost parallel to the abscissa.

(d) Obtained Values

The thickness of the diamond specimen in Fig. 8, for example, was measured to be 304 μm . Since the dispersion correction term is negligibly small in the case of diamond, the line connecting the crosses was obtained almost parallel to the abscissa, indicating no λ -dependent variation of the structure factors. Accordingly, the $|F'_{111}|^2$ values corresponding to the 11 crosses were almost the same, i.e. 5.56, and $f_{111} = (f_{111}^0 + f') \exp(-M)$ was found to be 3.23 in this experiment. Contrary to this, as shown in Fig. 9, a clear λ dependence of f_{hkl} has been obtained for heavier atoms. The λ dependence is attributed to the character of the anomalous dispersion term f' in the equation ($f_{hkl} = f_{hkl}^0 + f') \exp(-M)$. Cromer (1965) calculated f' for

Table 1. Absolute atomic scattering factors of Al and Cu

<i>hkl</i>	Al				Cu			
	Sp. No.	Thickness (μm)	f_{hkl}^0	Average f_{hkl}^0	Sp. No.	Thickness (μm)	f_{hkl}^0	Average f_{hkl}^0
111	1	512	8.816	$8.90_1 \pm 0.03$	1	89.7	21.61	21.80 ± 0.06
	2	444	8.892		2	96.0	21.80	
	3	448	8.951		3	116.7	21.96	
	4	430	8.982		4	74.6	21.84	
	5	419	8.896		5	63.9	21.78	
	6	345	8.892					
	7	304	8.880					
200	3	448	8.508	$8.52_2 \pm 0.05$	1	89.7	19.87	20.28 ± 0.11
	5	419	8.453		2	96.0	20.27	
	6	345	8.605		3	116.7	20.45	
					4	74.6	20.45	
					5	63.9	20.38	
220	1	512	7.314	$7.36_4 \pm 0.03$	1	89.7	16.62	16.75 ± 0.08
	2	444	7.387		2	96.0	16.89	
	3	448	7.404		3	116.7	16.97	
	4	430	7.335		4	74.6	16.71	
	6	345	7.312		5	63.9	16.58	
	7	304	7.430					
311	1	512	6.667	$6.66_5 \pm 0.02$	1	89.7	14.65	14.74 ± 0.04
	2	444	6.635		2	96.0	14.79	
	3	448	6.691		4	74.6	14.70	
	6	345	6.679		5	63.9	14.80	
	7	304	6.655					
222	1	512	6.444	$6.50_3 \pm 0.03$	1	89.7	14.40	14.36 ± 0.06
	2	444	6.555		2	96.0	14.37	
	3	448	6.508		4	74.6	14.47	
	6	345	6.446		5	63.9	14.19	
	7	304	6.564					
331	1	512	5.301	$5.33_3 \pm 0.02$				
	2	444	5.363					
	7	304	5.336					
400					1	89.7	12.30	12.46 ± 0.06
					2	96.0	12.50	
					4	74.6	12.57	
					5	63.9	12.48	
420	1	512	5.132	$5.14_4 \pm 0.03$				
	2	444	5.186					
	6	345	5.113					
422	2	444	4.663	$4.71_9 \pm 0.04$				
	6	345	4.721					
	7	304	4.773					

various elements by using relativistic Dirac-Slater wavefunctions. His values for C, Al, Si, Cu and Ge are also represented in Fig. 9, and show a λ dependence as close as that for the measured f_{111} . The absolute scattering factor f_{hkl}^0 can be evaluated from the measured f_{hkl} values by using

$$f_{hkl}^0 = \frac{1}{N} \sum_{n=1}^N \{f_{hkl} / \exp(-B \sin^2 \theta / \lambda^2) - f'(\lambda)\}, \quad (4)$$

where N is the number of observed extremum positions of hkl Pendellösung beats. As an example, Table 1 shows f_{hkl}^0 values of Al and Cu obtained for several different specimens with different thicknesses. Our average values of f_{hkl}^0 are compared with other values measured and calculated by various techniques and assumptions. A detailed discussion has been given in the original papers (Takama and Sato 1981; Takama *et al.* 1982).

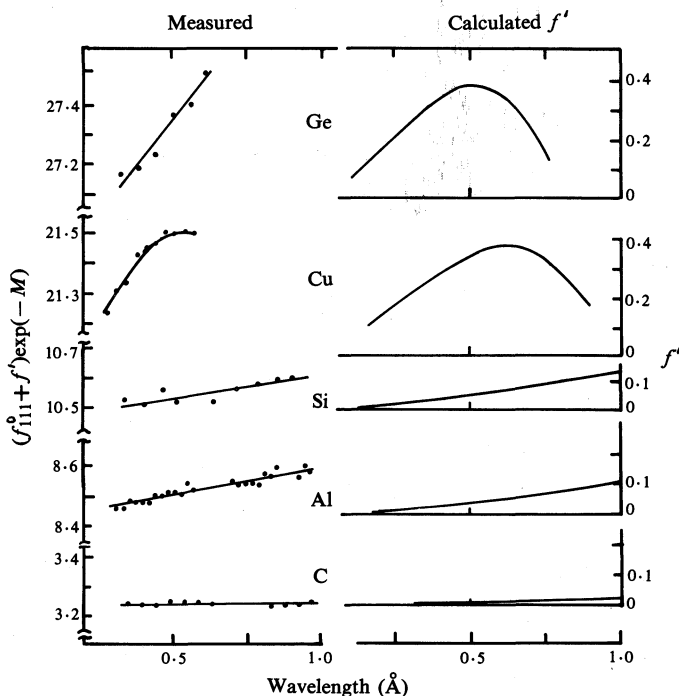


Fig. 9. Variations in the measured atomic scattering factors with wavelength. The wavelength dependence of the dispersion terms f' calculated by Cromer (1965) are also shown on the right.

(e) Errors

In the present method errors are possibly introduced in the determination of (1) the specimen thickness, (2) the wavelength and (3) the extremum positions in the beats, each of which is now discussed in detail.

(1a) Measurement using a micrometer: Since the micrometer used has a vernier scale of $1\ \mu\text{m}$, the fractional error in the thickness measurement will be $3\text{--}5 \times 10^{-3}$ depending on the absolute thickness, $0.2\text{--}0.3\ \text{mm}$. Moreover, only the thick part of the specimen will be measured if it has a non-uniform thickness. Therefore, smaller values of the structure factor or atomic scattering factor are possible in this method. Thus, the specimen surface should be as smooth as possible.

(1b) Measurement of attenuation of X rays: The absorption coefficients so far reported often have large errors, for example, a μ/ρ of Cu for Mo $K\alpha$ with $\pm 2\%$ (Hubbell *et al.* 1974). This will give rise to the same error in the values of the specimen thickness as well as the structure factor. In addition, the statistical errors

in the measured incident and transmitted intensities, I_e and I_t , can also induce an error in the thickness measurement. The error Δt in the thickness is expressed as $\Delta(I_t/I_e)/(I_t/I_e) = -\mu\Delta t$. The intensity ratio is usually measured with an accuracy of 1%, so that $\Delta t/t$ is estimated to be $1-2 \times 10^{-3}$ depending on the absolute value of the specimen thickness.

(2) The value of the photon energy E , which is related to the channel number η of the MCA by the equation $E = A\eta + B$, is calibrated by using several γ -ray and X-ray emission lines. The constants A and B are determined within an accuracy of 1×10^{-3} .

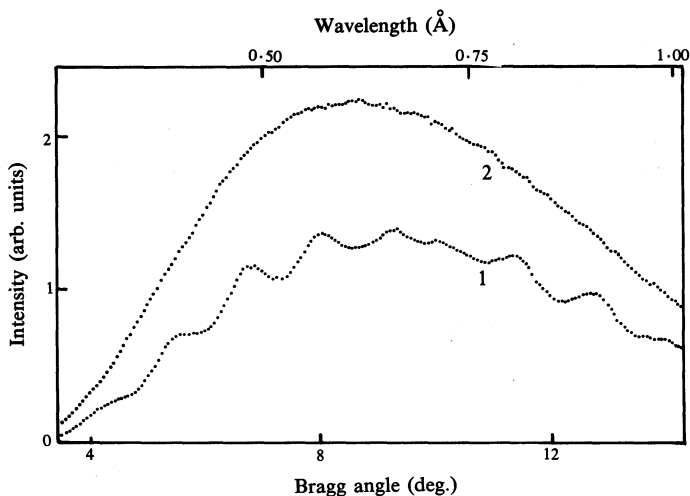


Fig. 10. Measured intensity variations from the diamond specimen in Fig. 3. Curve 1 is obtained from a dislocation free region (black square in Fig. 3), while curve 2 is from the region containing a large amount of dislocations (white square).

(3) The error $\Delta\lambda$ in the determination of extremum positions of beats depends upon the measured total intensities of the hkl reflection. Since the contribution of anomalous dispersion increases as the wavelength approaches the absorption edge, even though the total count is sufficient from the statistical point of view, the effective intensities in the beats, which determine the extremum position, decrease with wavelength, and hence the error increases in the long wavelength range, especially for heavy atoms. Similarly, the amplitude of beats in the fading region is too small to measure the extremum positions and the values from this region are usually excluded from the data to evaluate f_{hkl}^0 . The errors ΔE and $\Delta\lambda$ in (2) and (3) are related to the error $\Delta|F'_{hkl}|$ as

$$\Delta|F'_{hkl}|/|F'_{hkl}| \approx -\Delta\lambda/\lambda = \Delta E/E. \quad (5)$$

The error due to the determination of extremum positions can also be estimated, for example, from the scattering of the measured points around the lines in Fig. 9. The scattering is less than $\pm 1\%$ in this case and the amount of error in f_{hkl}^0 can be reduced by the averaging procedure in equation (4).

The incident radiation is assumed to be unpolarised in the present treatment. However, as Slivinsky (1971) has reported, white radiation emitted by commercial X-ray tubes with thick targets is usually polarised depending upon the photon energy and applied voltage. Olsen *et al.* (1978) have made a quantitative measurement of polarisation for copper and tungsten tubes and reported a diagram showing the amount of polarisation as a function of the ratio of photon to electron energy. We have checked the effect of polarisation on some of the experimental data in the structure factor determination using their diagram. A calculation showed that the shift of extremum positions due to polarisation was marked in the fading region. Nevertheless, the effect of polarisation on the measured values of structure factor was 3×10^{-3} at most.

What one measured in the present method is one of the typical dynamical diffraction phenomena, and hence, the single crystal specimen should be perfect enough to use the dynamical theory. As a preliminary survey to check the effect of defects, we tried to measure the beats of a diamond crystal from a region containing a large amount of dislocations and to compare these with those from a dislocation free region. Fig. 10 shows the resultant curves indicating a clear difference between the two measurements. Curve 1 is for the black square in Fig. 3, and curve 2 for the white square. One clearly sees a remarkable increase in total intensity accompanying the disappearance of Pendellösung beats in curve 2. Nevertheless, since the f_{hkl}^0 values obtained from the defect-free regions of different specimens are almost the same, we believe that the effect of the defects is not serious, provided that the irradiated region is strictly selected using the topographic method.

4. Method 2

(a) Intensity Distribution

It is expected in Fig. 1c that the intensity variation due to the wavelength change could be measured most effectively at TT' on the exit surface. In fact, in a preliminary test, the variation was detected to be more sensitive than in Method 1. The spherical wave theory of dynamical diffraction for absorbing crystals (Kato 1968a; Wada and Kato 1977) shows that the intensity I_{hkl} of the Bragg reflection on the exit surface of the specimen in the symmetrical Laue case can be expressed, assuming unpolarised incident X-rays, as

$$I_{hkl} = A(|\alpha|/\pi\zeta) \exp(-\mu t/\cos\theta) [\cos(2\alpha^r\zeta - \frac{1}{2}\pi) + \cosh(2\alpha^i\zeta) + |\cos 2\theta| \{ \cos(2\alpha^r\zeta |\cos 2\theta| - \frac{1}{2}\pi) + \cosh(2\alpha^i\zeta |\cos 2\theta|) \}], \quad (6)$$

where

$$\zeta = \sin\theta t(1-p^2)^{\frac{1}{2}}, \quad \alpha = (e^2/mc^2)2\lambda(F_{hkl}F_{\bar{h}\bar{k}\bar{l}})^{\frac{1}{2}}/V \sin 2\theta, \quad (7)$$

and where α^r and α^i are real and imaginary parts of α , A is a constant, $p = \tan\epsilon/\tan\theta$, with ϵ the angle shown in Fig. 11.

Equation (6) indicates that the intensity at the centre of the Borrmann fan, i.e. at $p = 0$, oscillates with $\alpha^r\zeta$ and $|\cos 2\theta|\alpha^r\zeta$ for the normal and parallel components of

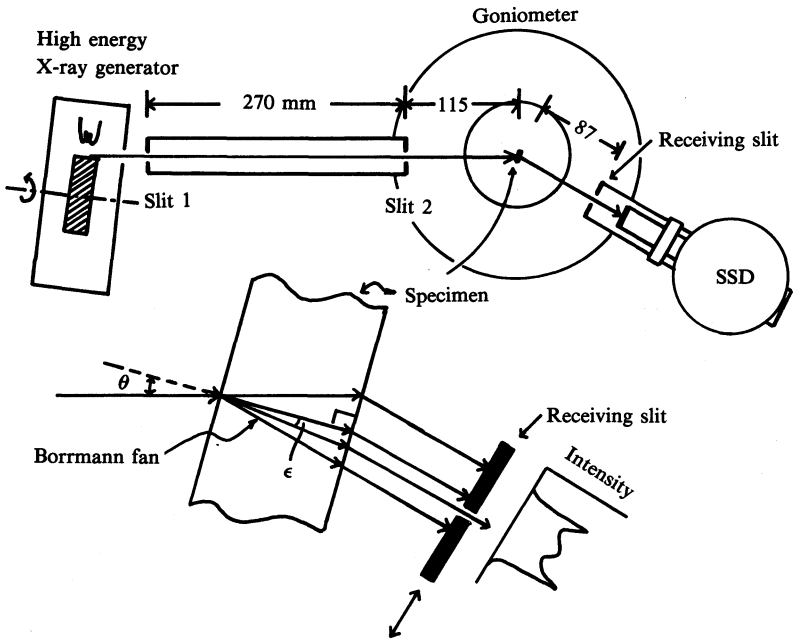


Fig. 11. Geometry of X-ray collimation in Method 2: slits 1 and 2 are $0.1 \times 3.0 \text{ mm}^2$ and the receiving slit is $0.05 \times 2.0 \text{ mm}^2$.

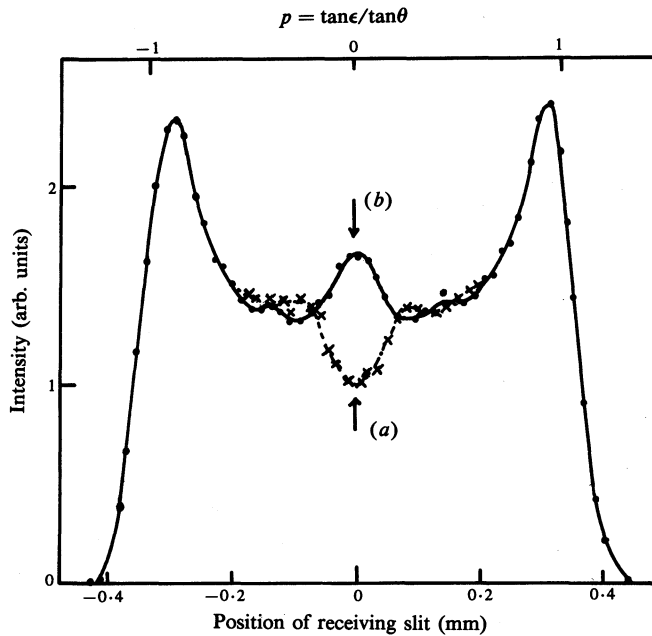


Fig. 12. Examples of the measured intensity distributions on the exit surface for the 220 reflection: (a) $\theta = 5.60^\circ$ ($\lambda = 0.375_1 \text{ \AA}$) and (b) $\theta = 5.66^\circ$ ($\lambda = 0.379_1 \text{ \AA}$). The arrows indicate a substantial difference in the diffracted intensities at $p = 0$ with two neighbouring θ settings.

polarisation respectively. Since $\alpha^r \zeta$ can be expressed at $p = 0$ as

$$\alpha^r \zeta = (e^2/mc^2) \{ (F_{hkl} F_{\bar{h}\bar{k}\bar{l}})^{\frac{1}{2}} \}^r \lambda t / V \cos \theta, \quad (8)$$

I_{hkl} oscillates with $\lambda t / \cos \theta$. Since the wavelength can be determined simultaneously with the intensity in the present technique, one obtains the values of $\{ (F_{hkl} F_{\bar{h}\bar{k}\bar{l}})^{\frac{1}{2}} \}^r$ accurately from the positions of the measured intensity extrema.

(b) Measurement and Results

The system of the intensity measurement is the same as in Method 1. However, a strictly collimated line-shaped beam $0.1 \times 3.0 \text{ mm}^2$ in size from a high energy X-ray generator (RIGAKU RU-1000C2: 120 kV, 20 kW) is utilised to measure the intensity only at the centre of the Borrmann fan on the exit surface from a thick crystal, as shown in Fig. 11. Fig. 12 shows an example of the measured difference in the intensity distribution on the exit surface for the 220 reflection of Si 3.363 mm thick. The curve (a) was obtained at $\theta = 5.60^\circ$ ($\lambda = 0.375 \text{ \AA}$) and (b) at $\theta = 5.66^\circ$ ($\lambda = 0.379 \text{ \AA}$). One sees a difference in intensity only near the centre of the Borrmann triangle. In Method 2, accordingly, the crystal is mounted at the centre of a goniometer so as to preserve the symmetrical Laue condition during the rotation changing θ around the vertical axis of the goniometer. For each θ position the intensity of the diffracted beam out of the exit surface is successively measured only at the centre by moving a narrow receiving slit $0.05 \times 2.0 \text{ mm}^2$ in front of the SSD, as shown in Fig. 11.

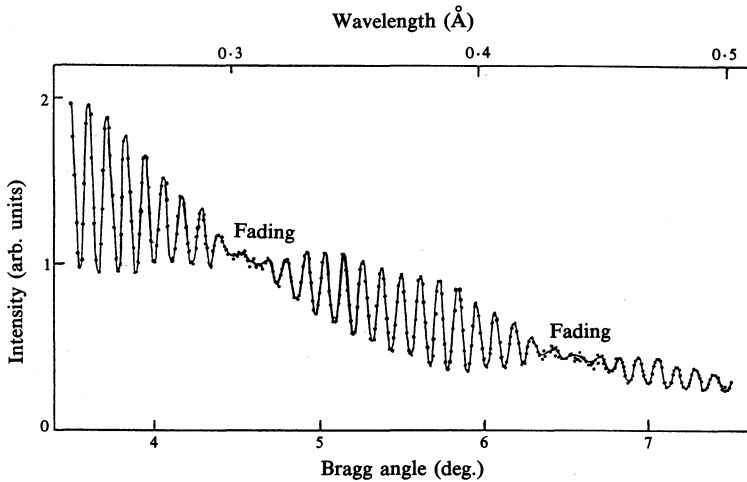


Fig. 13. Example of the Pendellösung beats measured by Method 2 for Si with $t = 3.478 \text{ mm}$ and the 220 reflection.

Fig. 13 shows an example of the Pendellösung beats obtained for the 220 reflection from a thick Si single crystal. Each point corresponds to the measured intensity for one θ setting diffracted at $p = 0$ in Fig. 12. One sees clear beats with a high frequency as well as with a large amplitude. The former results from the large specimen thickness, and the latter from the intensity measurement made only at $p = 0$, whereas in Method 1 the whole area underneath the curves in Fig. 12 has been measured.

Since the beats are very clear, one can determine the Bragg angle at the intensity extrema with an error $\Delta\theta < 0.005^\circ$. This error was estimated from the two measurements on both sides of the reflections 220 and $\bar{2}20$. The fractional error in determining the structure factors due to $\Delta\theta$ can be expressed approximately as $\Delta F_{hkl}^r / F_{hkl}^r = -2\Delta\theta / \sin 2\theta$ from equation (8), and for the 220 reflection the value is $< 1 \times 10^{-3}$ at $\theta = 6^\circ$. The thickness was 3.478 mm with an error of about 3×10^{-4} , neglecting the possible lack of uniformity in the irradiated region.

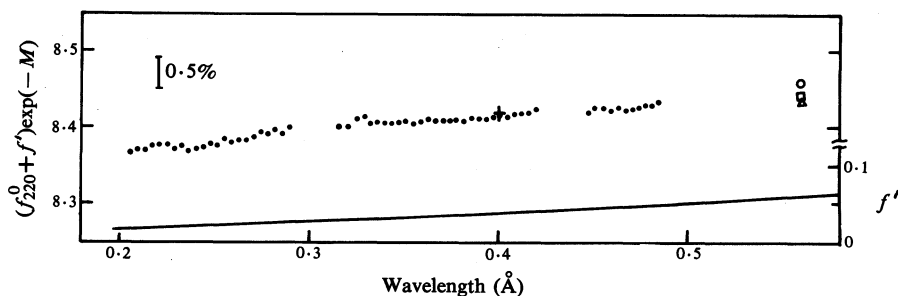


Fig. 14. Atomic scattering factor of Si from the beats in Fig. 13. The data so far reported are plotted for comparison: square, Hart and Milne (1969); open circle, Tanemura and Kato (1972); triangle, Aldred and Hart (1973); and cross, Saka and Kato (1986). The solid line shows f' calculated by Cromer (1965).

Fig. 14 shows the atomic scattering factor $(f_{220}^0 + f') \exp(-M)$ obtained from the beats in Fig. 13. One sees an approximately linear wavelength dependence close to that calculated by Cromer (1965). Values obtained by others are plotted for comparison.

5. Summary

The distinctive character of the present methods are summarised as follows:

- (1) No absolute intensity measurement is necessary.
- (2) Parallel-sided specimens can be used without any shaping procedure.
- (3) A tiny crystal such as a whisker can be used (Method 1).
- (4) A small region free from defects is selected to be irradiated (Method 1).
- (5) A large number of reflections are measured from the same area in the specimen.
- (6) The values of F_{hkl} or f_{hkl} automatically involve the wavelength-dependent character.
- (7) A desired wavelength range can be selected for various studies on anomalous dispersion.
- (8) A large number of beats can be obtained (Method 2).
- (9) Clear beats with a large amplitude are measured (Method 2).
- (10) A thick perfect crystal should be used (Method 2).

The effect of various kinds of defect on the beats should be systematically examined in detail. As a first step, a study on the effect of elastic bending strain is now under way.

Acknowledgments

The authors are greatly indebted to Professor N. Kato for his valuable comments. They also wish to acknowledge the experimental assistance made so far by students in our laboratory. The work was partly supported by the Grant-in-Aid for Scientific Research from the Ministry of Education, Science and Culture, in Japan (SS No. 57460173, TT No. 59550002, TT No. 62460224).

References

- Aldred, P. J. E., and Hart, M. (1973). *Proc. R. Soc. London A* **332**, 223–38.
- Aristov, V. V., Shmytko, I. M., and Shulakov, E. V. (1977). *Acta Cryst. A* **33**, 412–18.
- Batterman, B. W., Chipman, D. R., and DeMarco, J. J. (1961). *Phys. Rev.* **122**, 68–74.
- Buras, B., Olsen, J. S., Gerward, L., Selsmark, B., and Andersen, A. L. (1975). *Acta Cryst. A* **31**, 327–33.
- Cromer, D. T. (1965). *Acta Cryst.* **18**, 17–23.
- DeMarco, J. J., and Weiss, R. J. (1965). *Acta Cryst.* **19**, 68–72.
- Hart, M., and Milne, A. D. (1969). *Acta Cryst. A* **25**, 134–8.
- Hashimoto, H., Kozaki, S., and Ohkawa, T. (1965). *Appl. Phys. Lett.* **6**, 16–17.
- Hattori, H., Kuriyama, H., Katagawa, T., and Kato, N. (1965). *J. Phys. Soc. Jpn* **20**, 988–96.
- Hubbell, J. H., McMaster, W. H., Grande, N. K. D., and Mallett, J. H. (1974). 'International Tables for X-ray Crystallography', Vol. IV, pp. 45–70 (Kynoch Press: Birmingham).
- 'International Tables for X-ray Crystallography' (1962). Vol. III (Kynoch Press: Birmingham).
- James, R. W. (1967). 'The Optical Principles of the Diffraction of X-rays' (Bell: London).
- Kato, N. (1955). *J. Phys. Soc. Jpn* **10**, 46–55.
- Kato, N. (1961). *Acta Cryst.* **14**, 526–32.
- Kato, N. (1968 *a*). *J. Appl. Phys.* **39**, 2225–30.
- Kato, N. (1968 *b*). *J. Appl. Phys.* **39**, 2231–7.
- Kato, N., and Lang, A. R. (1959). *Acta Cryst.* **12**, 787–94.
- Kozaki, S., Ohkawa, T., and Hashimoto, H. (1968). *J. Appl. Phys.* **39**, 3967–76.
- Olsen, J. S., Buras, B., Jensen, T., Alstrup, O., Gerward, L., and Selsmark, B. (1978). *Acta Cryst. A* **34**, 84–7.
- Saka, T., and Kato, N. (1986). *Acta Cryst. A* **42**, 469–78.
- Slivinsky, V. W. (1971). *Bull. Am. Phys. Soc.* **16**, 546.
- Takama, T., Iwasaki, M., and Sato, S. (1980). *Acta Cryst. A* **36**, 1025–30.
- Takama, T., Kobayashi, K., Hyugaji, M., Nittono, O., and Sato, S. (1984 *a*). *Jpn J. Appl. Phys.* **23**, 11–14.
- Takama, T., Kobayashi, K., and Sato, S. (1982). *Trans. Jpn Inst. Met.* **23**, 153–60.
- Takama, T., Kobayashi, K., Tohno, S., and Sato, S. (1984 *b*). *Acta Cryst. A* **40**, C347.
- Takama, T., Noto, N., Kobayashi, K., and Sato, S. (1983). *Jpn J. Appl. Phys.* **22**, L304–6.
- Takama, T., and Sato, S. (1981). *Jpn J. Appl. Phys.* **20**, 1183–9.
- Takama, T., and Sato, S. (1982). *Philos. Mag. B* **45**, 615–26.
- Tanemura, S., and Kato, N. (1972). *Acta Cryst. A* **28**, 69–80.
- Wada, M., and Kato, N. (1977). *Acta Cryst. A* **33**, 161–8.